Journal of Power Sources 226 (2013) 256–265

Contents lists available at SciVerse ScienceDirect

Journal of Power Sources

journal homepage: www.elsevier.com/locate/jpowsour

High temperature stabilization of lithium–sulfur cells with carbon nanotube current collector

Hyea Kim, Jung Tae Lee, Gleb Yushin*

School of Materials Science and Engineering, Georgia Institute of Technology, Atlanta, GA 30332, USA

HIGHLIGHTS

- The effect of high temperature on the Li–S cell performance was investigated.
- When operating at 70 °C the cells demonstrated the best rate capability and capacities.
- SEM/EDS studies revealed thicker SEI on the Li anode surface at higher temperatures.
- Thicker SEI prevented polysulfides diffusion and their irreversible reduction into Li_2S.
- The increase in inorganic components of the SEI suppressed the Li dendrite growth.

ARTICLE INFO

Article history:
Received 17 August 2012
Received in revised form
3 October 2012
Accepted 11 October 2012
Available online 2 November 2012

Keywords:
Li–S
Li ion battery
Carbon nanotube
Temperature
Nanocomposite
Cathode

ABSTRACT

Lithium–sulfur (Li–S) chemistry has been considered for an alternative future generation of rechargeable lithium batteries because of its higher theoretical capacity, safer operation and lower material cost. Here, we report on the impact of temperature on Li–S cell performance. The Li–S coin-cells were prepared by using S infiltrated vertically aligned carbon nanotube arrays (S-CNT) as cathodes and lithium metal foils as anodes. The cells were operated at 25, 50, 70 and 90 °C. Higher temperature operation resulted in higher specific capacity, better rate capability and more stable performance. Scanning electron microscopy (SEM), energy dispersive spectroscopy (EDS) and electrochemical impedance spectroscopy (EIS) studies reveal the major impact of temperature on the solid electrolyte interphase (SEI) on Li foil. Thicker SEI with higher content of inorganic phase formed at elevated temperatures greatly reduced both the dendrite formation and the capacity fading resulted from the irreversible losses of S. At 70 °C specific capacities up to ~700 mAh g^{-1} were achieved at an ultra-high current density of 3.3 A g^{-1}. At 90 °C and the same current density Li–S cells showed an average capacity of ~400 mAh g^{-1} and stable performance for over 150 cycles.

1. Introduction

Lithium ion batteries (LiBs) have being serving as power sources for various portable devices such as laptops, smart phones and electric vehicles. However, ever-rising power demands for these devices have surpassed the current technology of LiB. The specific energy of the commercialized LiB has become insufficient due to the relatively low capacity of the electrode materials [1] and the growth in the energy density of LiB has reached the stagnation.

In order to increase the energy density of the LiB, new electrode materials with higher gravimetric and volumetric capacities should be developed [2–7]. There have been some improvements in the developments of high capacity silicon (Si)-based anodes, which offer over several times higher capacity than the traditional graphite anodes and are produced of similarly low cost and abundant materials [8–18]. To maximize the advantages of Si-based anodes, however, one needs to develop cathode materials with comparably high volumetric capacity. Such developments, however, have shown smaller progress.

Sulfur (S)-based materials are considered to be attractive candidates for the next generation cathodes due to the very low cost and abundance of S in nature combined with enhanced safety associated with the use of low-voltage cathode materials [19–36]. Sulfur offers very high theoretical gravimetric capacity of 1672 mAh g^{-1}, which is an order of magnitude higher than state of the art commercial electrodes. The volumetric capacity of S-based electrodes depends on the electrode microstructure and porosity, but even if S occupies 33% of the electrode volume (the rest being

* Corresponding author.
E-mail address: yushin@gatech.edu (G. Yushin).

0378-7753/$ – see front matter © 2012 Elsevier B.V. All rights reserved.
http://dx.doi.org/10.1016/j.jpowsour.2012.10.028

reserved for the carbon additives and the pre-existing porosity) and the S utilization is 90%, it may easily approach ~1000 mAh cc^{-1}, which is about two times higher than that of commercial cathodes.

Yet there are several challenges preventing commercialization of S cathodes for the next generation lithium batteries. The largest challenge is an extensive capacity degradation occurring during cycling because of the high solubility of some of the polysulfides (such as Li_2S_8 or Li_2S_4, reaction intermediates during discharge) in electrolytes [23,35,36]. This dissolution also leads to the self-discharge and to the eventual precipitation of electrically insulative and insoluble Li_2S_2 and/or Li_2S onto the surface of both electrodes during the battery operation, which commonly further limits the cell performance. Such deposits may contribute to the permanent losses of the active material (Li and S) and to the increased ionic resistance of the cell, as the deposits partially block the ion transport. The dissolution of polysulfides and their re-deposition on the cathode surface is often referred to as a "shuttle mechanism" [23,37]. While the cathode dissolution is often considered to be highly undesirable, a well-controlled "shuttle mechanism", involving fully reversible dissolution and re-deposition of polysulfides on the surface of conductive cathodes could be a viable option if a barrier could be built to prevent polysulfides from reaching the anode and forming insoluble precipitates.

Another challenge is highly electronically insulating properties of S, which require the uniform introduction of electrically conductive material, such as carbon and conducting polymers, into the electrode in order to improve the utilization of S [19–21,24,28–35].

Finally, Li-free low-voltage cathodes require the use of Li-containing low-voltage anodes, which may increase the overall cost of LiB production because of the need to use more expensive production facilities. The use of metal Li as an anode does carry some benefits too. Its low potential and very high volumetric and gravimetric capacities can maximize the energy density of lithium–sulfur (Li–S) cells. In conventional LiBs, Li anodes are never used because they form dendrites during repeated Li plating-dissolution cycles, which eventually result in an internal short circuit. With S cathodes, however, some of such issues can be mitigated. The formation of electrically isolative Li_2S may self-limit the short circuit reaction processes, while some of the polysulfides deposited on Li may suppress the dendrite formations.

Many of the key Li–S processes governing the cell performance, including the polysulfide dissolution rate, the ionic transport and the solid electrolyte interphase (SEI) on the Li foil, shall be thermally activated. Surprisingly, we could not find any systematic studies on the effects of cell operating temperature. Therefore, in this work we were interested to reveal how this temperature may impact the performance of Li foil-S cells, where the dissolution of the polysulfides is not restricted by S incorporation in a porous matrix [24,29,38,39] or by surface coating of S particles with various barriers for solvent and polysulfide molecules. In order to achieve high electrical connectivity within the S electrode, we have utilized vertically aligned carbon nanotubes (VACNTs), which have recently shown great promises for high capacity anodes [40] and cathodes [41] due to their excellent thermal and electrical properties. In addition, high porosity of the VACNTs allow for uniform deposition of the active material. Due to high strength and excellent mechanical properties of CNTs, the compression of the VACNT-based electrodes to achieve higher volumetric capacity does not induce cracks or any other undesirable mechanical defects.

We observed the in-situ formation of a protective coating on a Li foil anode at elevated temperatures of 70–90 °C. At 90 °C, the Li–S cells with ~50 μm thick compressed VACNT/S electrodes could be charged and discharged within 6 min, while maintaining average capacity in the range of ~400 mAh g^{-1} and showing cycle life stability in excess of 150 cycles. The combination of high capacity, high rate performance and moderately high stability of the thick VACNT/S electrodes is unprecedented. While higher cycle stability

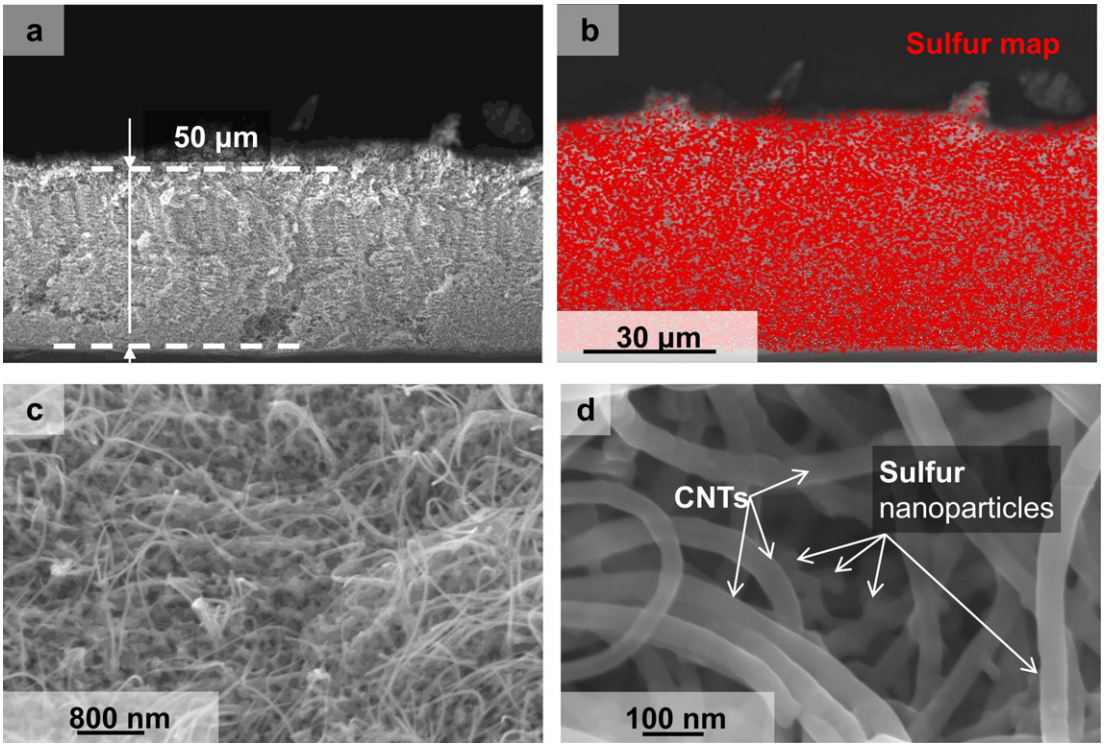

Fig. 1. Electron microscopy of S-CNT cathode. (a) SEM micrograph of the cross-section. (b) EDS mapping of the S distribution within the electrode superimposed on the SEM micrograph. (c, d) SEM micrographs of the top of the electrode recorded at different magnifications.

is strongly desired, our results additionally suggest a promise of an approach to form protective coatings on Li foil anodes in-situ at elevated temperatures.

2. Experimental

VACNTs were grown by a chemical vapor deposition (CVD) process at 850 °C using acetylene gas as a precursor, iron chloride as a catalyst and quartz as a substrate, as earlier described [40,42]. The 5 min deposition process yields VACNT forest of ~250 μm in thickness. The produced VACNTs have then been transferred to a nickel (Ni) foil current collector using a polyvinylidene fluoride (PVDF) adhesive interlayer, which was then carbonized at 700 °C (under compressive stress applied to the VACNT/PVDF/Ni sandwich) to improve the thermal stability of the CNT/Ni interface. This procedure decreased the VACNT electrode thickness and increased its density by around five times.

In our initial studies we attempted to infiltrate VACNT electrodes with S using a repeated solution infiltration procedure [19]. This method, however, did not allow us to achieve the desired composite uniformity within the electrode thickness. Much better results were achieved by dipping the VACNT electrodes in a molten S. The excess of S from both the electrode surface and from the bulk was removed by heating the electrode at 250 °C in air. The S evaporation time was adjusted to achieve 3:1 mass ratio of S:C. We estimate the statistical error in the mass measurements to be ~7%.

The coin-cells were assembled with the 1 M bis(trifluoromethanesulfonyl)imide (LiTFSI) in dimethoxyethane (DME):1,3-dioxane (DIOX) (1:1, v:v) [Alfa Aesar, 99%] as an electrolyte, celgard2325 (Celgard, USA) separator and pure Li foil [Alfa Aesar, 99.9%] anode. 0.2 M $LiNO_3$ [Alfa Aesar, 99.99%] was introduced to the electrolyte as an additive to improve the coulombic efficiency [43]. The electrodes (mass loading of ~1 mg cm^{-2}) were dried at 50 °C under vacuum overnight before assembly into coin-cells. The cells were equilibrated for 24 h before operation.

Electrochemical experiments were performed with Arbin battery test system (Arbin Instruments, USA). The coin-cells were assembled inside an Ar glove box (<1 ppm of H_2O, Innovative Technologies, USA) and cycled between 3.0 V and 1.2 V vs Li/Li^+ (V) in galvanostatic mode. The cells were evaluated with different C-rates at C/10, C/5, C/2, 1C, 2C, 5C and 10C, and then the durability test was continued at 2C for 400 cycles. The C-rates are calculated based on the mass of sulfur using a theoretical capacity of 1672 mAh g^{-1}. AC impedance was carried out with Solartron 1480 (Solartron Analytical, USA). The frequency of the impedance measurements ranged from 1 Hz to 10^6 Hz with an AC signal amplitude of 10 mV.

The morphology of the Li foils and VACNT/S electrodes after cycling at different temperatures were characterized by Nova 200 NanoLab (FEI, USA) at a beam voltage of 5 kV and a working distance of 4 mm. After cycling the cells were opened inside the glove box with <1 ppm water and the electrodes were washed with dimethyl carbonate (DMC) to remove residual salts and electrolyte. The samples were transferred from a glove box to the analysis chamber in a sealed pouch bag. The air exposure time was minimized to ~3 min. Energy dispersive X-ray spectroscopy (EDS) was carried out with Zeiss Ultra60 FE-SEM to investigate the uniformity of S infiltration into VACNTs and to study the changes in the surface chemistry of the Li anode after cycles on around 1800 × 1200 μm^2 analysis area.

3. Result and discussion

The first issue in the fabrication of VACNT/S composite cathodes was to obtain uniform S distribution through the carbon matrix.

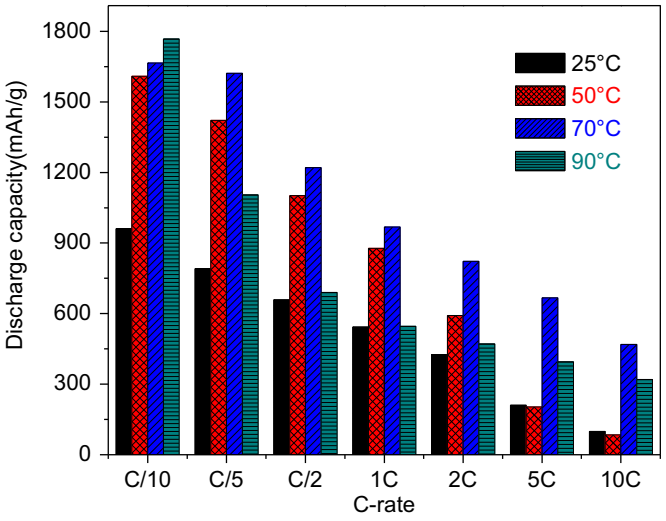

Fig. 2. Discharge capacity of S-CNT cathode as a function of C-rate and testing temperature. The capacity is normalized by the weight of S.

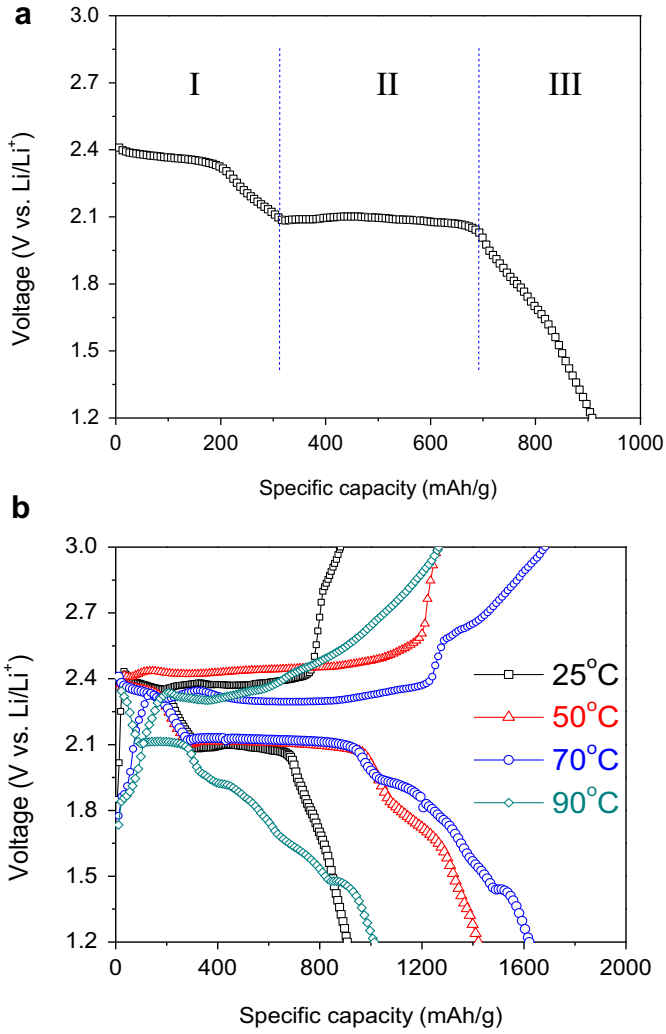

Fig. 3. Charge–discharge characteristics of an Li–S battery cell: (a) A typical voltage profile corresponding to a cell discharge and (b) the effect of temperature on the shape of the charge/discharge profiles at C/5.

Agglomerates of S can prevent lithium ions from transporting through the electrode. In addition, large S particles and their agglomeration may lack the sufficient electrical conductivity needed for electrochemical reactions. SEM microscopy showed an average CNT diameter of ~50 nm and very high uniformity of the VACNT/S electrodes. No agglomerates and no S particles larger than 500 nm were visible. Fig. 1a shows an example of SEM micrograph of the cross-section of the prepared VACNT/S cathode. The S infiltration process and the attachment of the VACNT/S electrode to a Ni current collector under pressure evidently reduced the electrode thickness from ~250 μm (height of the as-grown VACNTs) to ~50 μm. The uniformity of S infiltration was confirmed by EDS mapping (Fig. 1b). The majority of S nanoparticles has an intimate contract with CNTs and is of 20–100 nm in diameter (Fig. 1c, d). The uniform S distribution (Fig. 1b, c) and the uniform porosity of the produced electrodes shall be beneficial for high rate performance.

Fig. 2 summarizes the electrochemical rate testing in half cells as a function of temperature. At the slowest C-rate of C/10, the capacity of the VACNT/S cathode approached 960 mAh g^{-1} at 25 °C. However, upon increasing the temperature to 50–90 °C, the capacity was almost doubled and reached the theoretical value at 90 °C. Such a dramatic effect of temperature could be explained by the greatly improved ion transport at elevated temperatures. Here we would like to clarify that the capacity retention with increasing current density (increasing "C"-rate) was performed on the same electrode at a fixed temperature in a series of charge-discharge tests. As a result, Fig. 2 shows a combined effect of both the stability of the cathodes and its capacity retention with increasing current density. We would like to further clarify that the overall rate capability of the tested cells is limited not only by the ion and electronic transport with the cathode, but also by the Li transport through the solid electrolyte interphase (SEI) layer on Li and the overall Li dissolution/plating kinetics.

We expect the electrical connectivity within the cathode to be relatively independent on temperature. With increasing temperature several competing processes may take place. On one hand we expect faster ion transport through both the cathode and the SEI on Li foil. This shall increase the cell rate performance. On the other hand, higher temperature may also lead to faster rate of undesirable reactions, such as cathode dissolution and formation of S-based precipitates on the surface or within the SEI layer. This will contribute to both the capacity fading and increasing the ionic resistance, which shall reduce the rate performance.

The rate capability of the cells tested at all temperatures was moderately good. Increasing the current density from "C/10" (167 mA g_S^{-1}) to "1C" (1672 mA g_S^{-1}) in cells tested at 25 and 50 °C showed retention of 55–57% of capacity. However, further increasing current density to "10C" (~17 A g_S^{-1}) allowed extraction

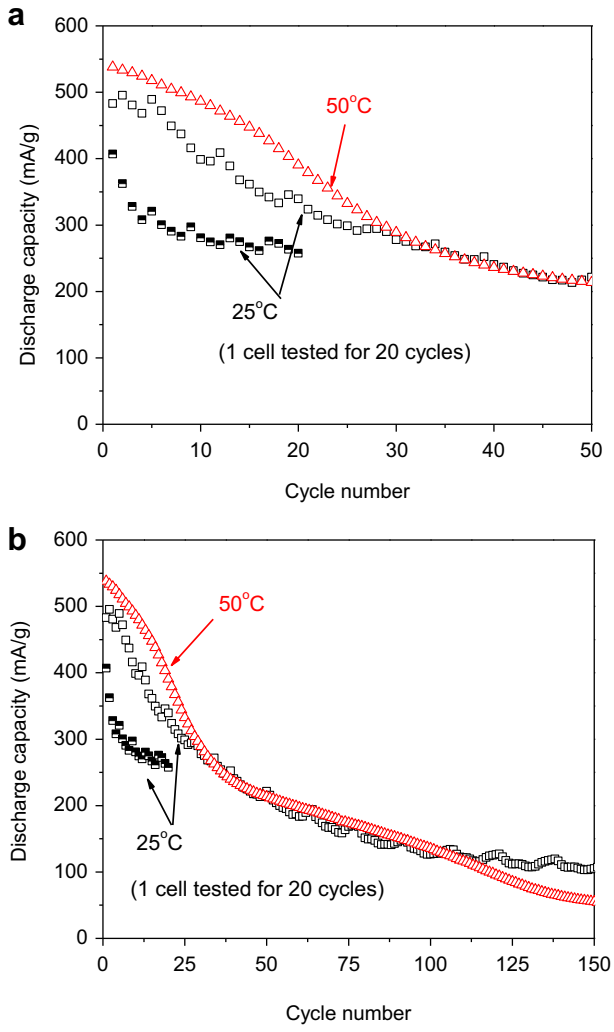

Fig. 4. The cycle stability of CNT-S cathodes tested at 2C current density at 25 and 50 °C: (a) the first 50 cycles, (b) the first 150 cycles. The capacity is normalized by the weight of S.

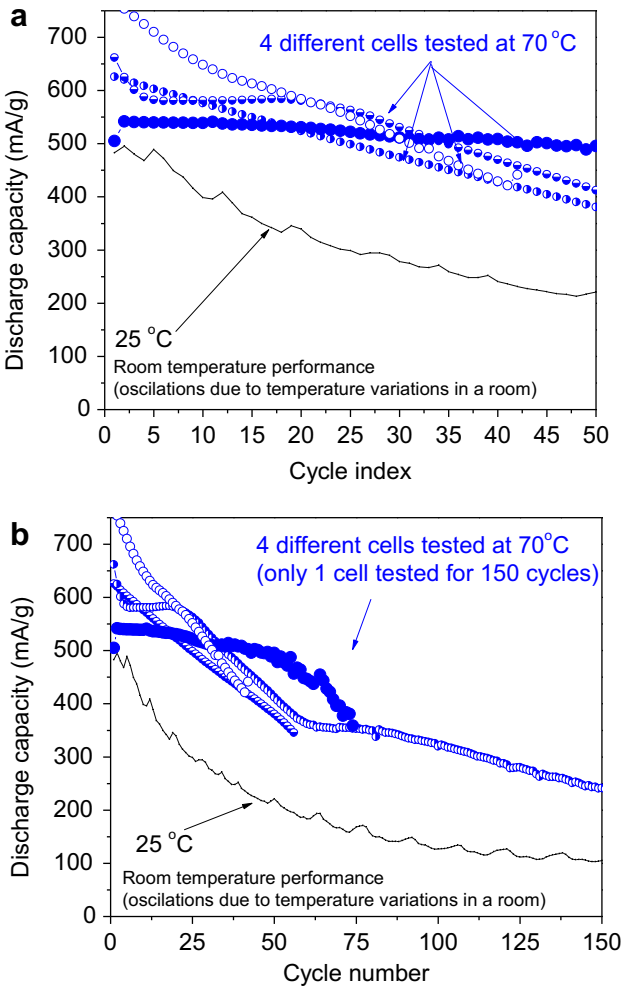

Fig. 5. The cycle stability of CNT-S cathodes tested at 2C current density at 70 °C: (a) the first 50 cycles, (b) the first 150 cycles. The capacity is normalized by the weight of S.

of only 5–10% of the total capacity at these temperatures. Interestingly, the higher temperature of 50 °C showed lower capacity at the highest current density. Since higher temperature may only increase the ion transport, these results suggest building a thicker layer of ionically resistive material on the Li foil anode at 50 °C. Increasing temperature to 70 °C resulted in the best rate capability, with ~60% maximum capacity at "1C" and ~30% at "10C". The demonstrated capacity of 470 mAh g_S^{-1} at ultra-high current density of ~17 A g_S^{-1} indicate a high promise of the Li–S chemistry to achieve a combination of the ultra-high specific capacity and rapid discharging capability. At this temperature an optimum balance of high ionic conductivity and moderately thick precipitate/SEI layer on Li was achieved. Increasing the temperature further to 90 °C showed only 30 and ~20% capacity retention at these rates, respectively.

To better understand the effect of temperature, the charge–discharge voltage profiles of the Li–S cells were investigated in Fig. 3. It is known that the Li–S battery shows two plateaus during discharge process (Fig. 3a) [23,35]. First upper plateau at ~2.4 V (vs. Li/Li^+) is believed to correspond to the redox reaction of high-order polysulfides soluble in the electrolyte (Li_2S_X, $4 \leq X \leq 8$, Fig. 3a region I), and the second major plateau at ~2.0 V is believed to correspond to the conversion of high-order to insoluble low-order polysulfides, Li_2S_2 (Fig. 3a region II) and finally to Li_2S (Fig. 3a region III).

Increasing temperature from 25 to 50 and 70 °C, the capacity increased mostly due to the longer second plateau at 2.1 V (Fig. 3b), suggesting increasing ability to achieve higher degree of lithiation with increasing diffusion coefficient of Li in polysulfides. Increasing the temperature also gradually increased the length of the region III (Fig. 3b). If this region represents the transformation of both the insoluble Li_2S_2 and soluble higher order polysulfides to insoluble Li_2S, this finding may indicate increased content of the lower potential Li_2S phase with increasing temperatures. Interestingly, further temperature increase to 90 °C (Fig. 3b) reduces region II and increases region III (Fig. 3a). Such behavior may be linked to the fast dissolution of the soluble polysulfides at such high temperature (thus smaller plateau) and earlier formation of the insoluble Li_2S on the cathode surface, which lowers its overall cathode potential. This rapid formation of Li_2S upon Li insertion into S may have both positive and negative consequences. On one hand, the low average discharge voltage of an Li–S cell with five separate plateaus observed at 90 °C lowers its energy density. On the other hand, if the formation of insoluble phases is enhanced, the cell stability and cycle life may be increased.

The voltage hysteresis between the charge and discharged plateau (Fig. 3b, region II) correlates with the cell rate performance

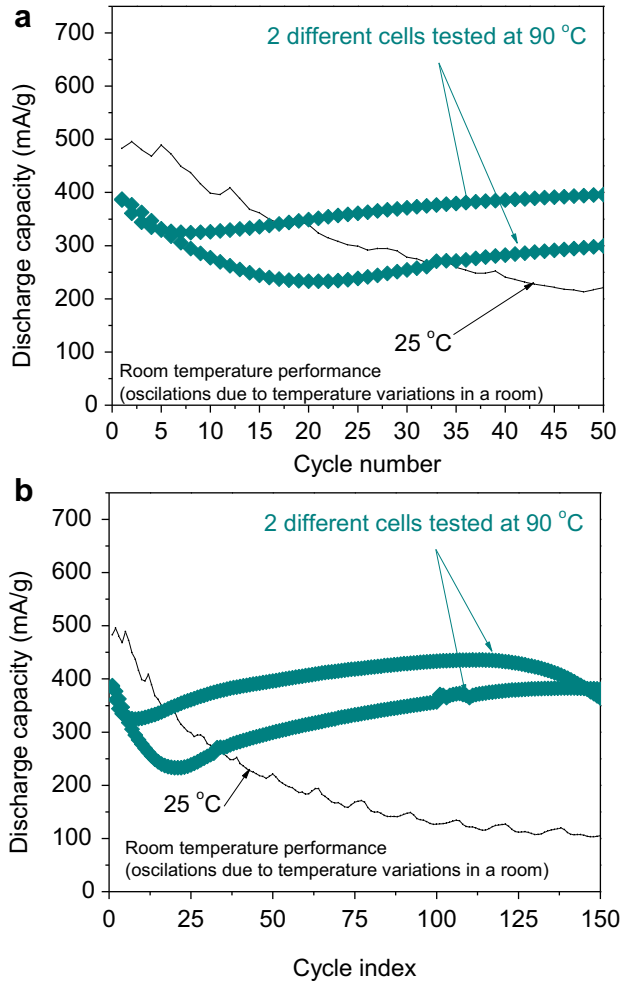

Fig. 6. The cycle stability of CNT-S cathodes tested at 2C current density at 90 °C: (a) the first 50 cycles, (b) the first 150 cycles. The capacity is normalized by the weight of S.

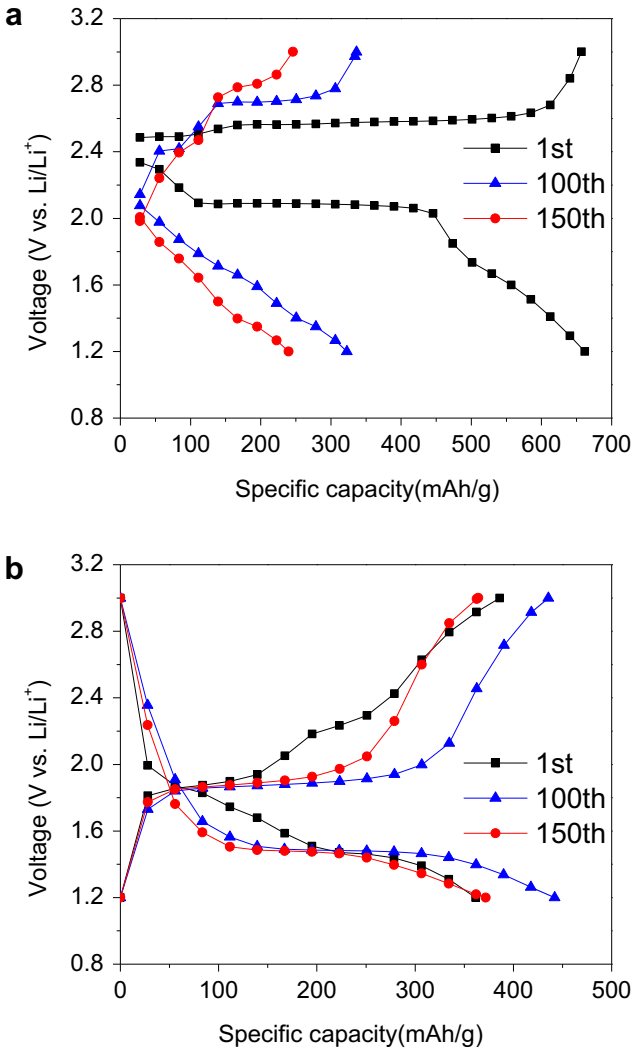

Fig. 7. Changes in the charge–discharge profiles of the CNT-S cathodes recorded at 2C current density with cycling at different temperatures: (a) 70 °C and (b) 90 °C. The capacity is normalized by the weight of S.

(Fig. 2). The largest hysteresis indicative of the highest IR losses (largest resistance) of 0.32 V is observed in a 50 °C cell and the smallest hysteresis of 0.18 V is observed in a 70 °C cell (Fig. 3b), supporting previously discussed hypothesis on the impact of temperature on the formation of precipitates/SEI on Li anode.

The cycle durability of the cells at elevated temperatures at a fixed C-rate of 2C is shown in Figs. 4–6. At room temperature and at 50 °C cells rapidly degrade starting from the first cycle. Less than 50% of the initial capacity is left after 50 cycles and only 5–10% after 150 cycles (Fig. 4). However, cells tested at 70 °C not only demonstrated higher specific capacity and better rate capability (Fig. 2), but also more stable performance (Fig. 5). In fact, one of the tested cells showed virtually no degradation within the first 50 cycles (Fig. 5a). Increasing the cell testing temperature further to 90 °C even better cycle stability was observed (Fig. 6). While the cells showed low capacity and degradation at the initial cycles, the prolonged cycling revealed a self-healing/self-improving behavior. After initial decline in the specific capacity for the first 5–20 cycles, these cells showed gradually increasing capacity till over 130–150 cycles. After 100 cycles, specific capacity in the excess of 400 mAh g_S^{-1} was achieved. Such a behavior was rather surprising because the cathode dissolution rate should be accelerated at elevated temperatures. Clearly some stabilization mechanism should be acting to counter-balance the irreversible cathode dissolution and the continuous formation of Li_2S_2 and/or Li_2S deposits on the Li anode surface at elevated temperatures.

In Fig. 7, the voltage profiles during cycles of the VACNT/S electrodes at 70 and 90 °C are compared. The typical second plateau at 70 °C disappeared as the capacity decreased during cycling (Fig. 7a). At 90 °C, in contrast, a plateau found at 1.5 V (Fig. 3) was clearly visible after 100 and 150 cycles (Fig. 7b). From the 1st cycle to 130th cycle, this plateau is becoming larger, demonstrating higher capacity and good stability of the corresponding redox reactions. However, it shows noticeably lower reduction/oxidation potential than at room temperature. The origin of this phenomenon is currently unclear and may be related to the reversible transformation of S directly into a lower voltage Li_2S.

In order to investigate the impact of the operation temperature on the formation of the Li_2S_2 and/or Li_2S deposits on the Li foil SEI we performed a series of SEM and EDS studies (Figs. 8–10). Figs. 8 and 9 show typical morphologies of SEI films formed on Li after cycling at different temperatures. The noticeable SEI film thickness

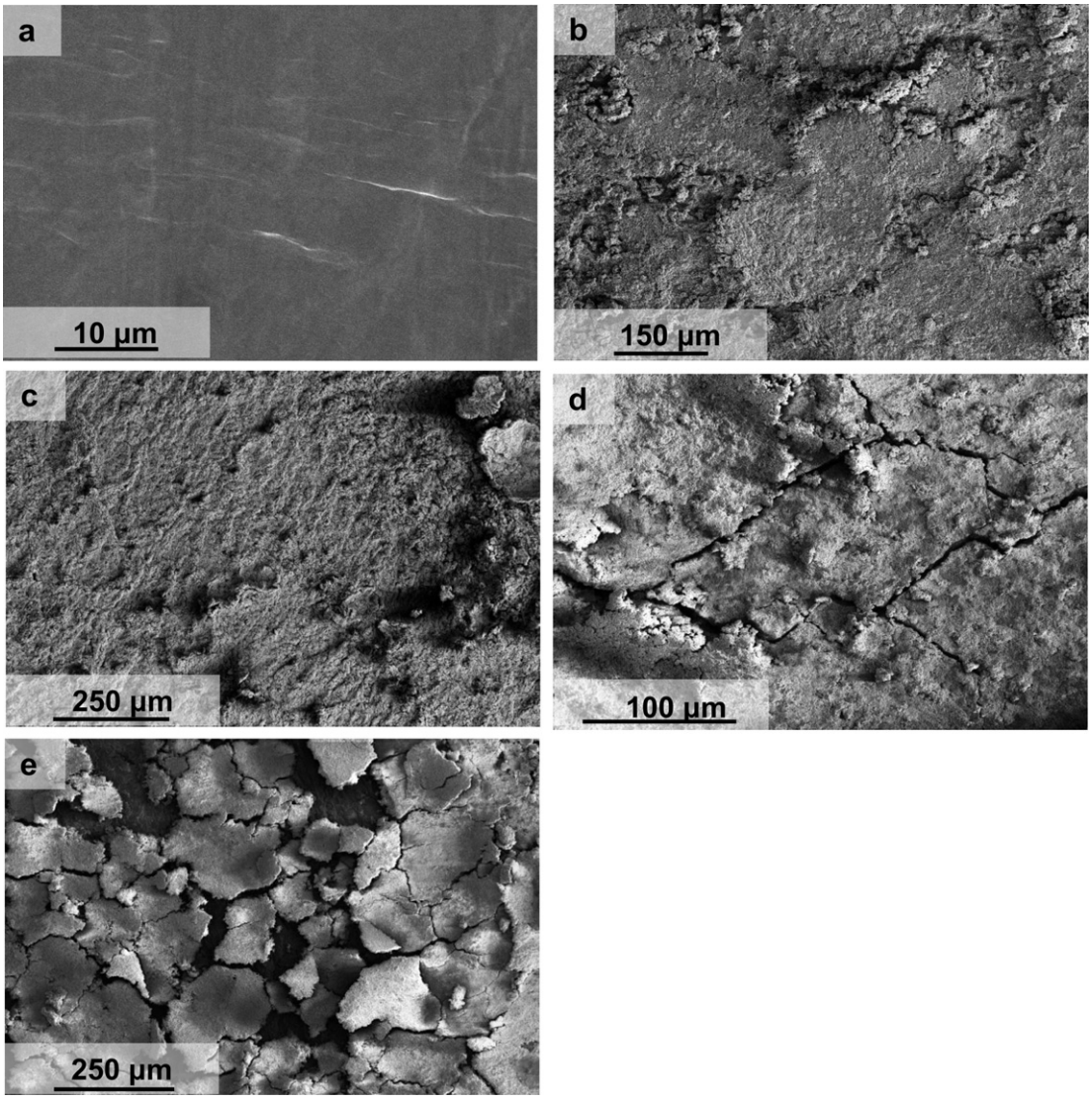

Fig. 8. SEM micrographs of (a) fresh lithium surface and the Li anode after cycling Li/S cells at (b) 25 (c) 50 (d) 70 and (e) 90 °C.

was observed in all samples, but was particularly visible at elevated temperatures. In cells cycled at 70 and 90 °C the adhesion between the Li metal and thick SEI was poor. As a result of larger SEI thickness, weaker adhesion, and larger thermal stresses between Li and the SEI (originating during the cell cool-down due to the differences in their thermal expansion coefficients), the Li anodes of the cells tested at higher temperatures showed higher degree of SEI cracking and its partial delamination from Li. We acknowledge that while Li electrode experiences large strain due to the volume changes throughout the Li insertion/desertion [44–46], many of the cracks observed in the SEI may be formed not in-situ, but during the coin cell disassembling and SEM sample preparation. The SEI thickness measured on delaminated SEI films was estimated to grow from ~15 μm at 70 °C to ~40 μm at 90 °C.

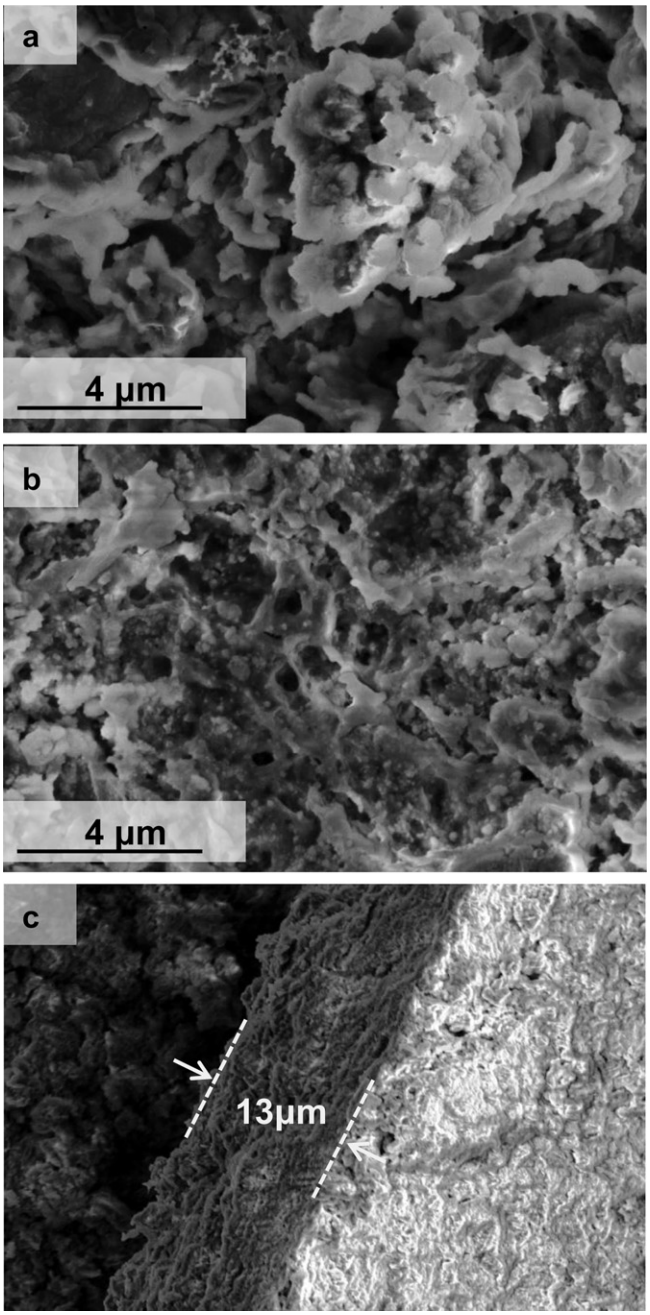

Fig. 9. SEM microscopes of Li anode: (a) dendrite structure formed at 25 °C, (b) reduced dendrite formation observed at 90 °C, (c) SEI thickness measured at 70 °C.

A significant difference in surface morphology of SEI on Li was found at different temperatures (Figs. 8 and 9). In cells cycled at 25 °C, the SEI has noticeably higher roughness (largest size of dendrites) than in cells cycled at the higher temperatures (compare Fig. 9a and b). Two phenomena maybe responsible for the smoother SEI in cells cycled at elevated temperatures. First, at temperatures close to a melting point (note that 90 °C or 363 K is 80% of Li melting point, 454 K) high mobility of atoms commonly lead to the greatly reduced formation of dendrites during reversible plating of metals. In fact, liquid metals virtually do not form dendrites upon repeated plating and metal ion extraction into liquid electrolyte. Second, formation of a rigid ionically permeable and electrically insulating SEI layer on the Li surface (such as an ex-situ or in-situ formed solid electrolyte layer) should also greatly reduce the dendrite formation. High magnification SEM revealed a net-like porous structure of the SEI formed at 90 °C (Fig. 9b).

The EDS results shown in Fig. 10 clearly indicate the chemical composition of SEI is dependent on a cell operation temperature. The SEI is expected to be composed of the electrolyte (1 M LiTFSI salt solution in DIOX:DME = 1:1 solvent mixture with the addition of 0.2 M $LiNO_3$) reduction products with the potential contribution of the low-order lithium polysulfides (Li_2S and Li_2S_2). From the $TFSI^-$ reduction, fluorine and sulfur containing compounds such as LiF, $LiCF_3$ and $Li_2S_2O_4$ are commonly produced [47]. Aurbach et al. further demonstrated that $LiNO_3$ addition to electrolyte resulted in the incorporation of Li_xNO_y and Li_xSO_y species (the last one via oxidation of various S containing compounds) into Li SEI surface and the greatly reduced amount of Li_2S component of the SEI [47]. The primary source of C in the EDS – reduced solvents; the sources of O – the products of electrolyte decomposition and the unavoidable short-term exposure to and oxidation of Li anodes in air during transferring samples to the SEM; the source of F-LiTFSI salt; the sources of S include reduction products of LiTFSI salt as well as S transferred from the cathode (LiS and Li_2S). As increasing the temperature, more F and S and less O were detected.

The greatly reduced O content observed in cells cycled at higher temperatures can be explained by thicker SEI layer (Figs. 8 and 9) and thus greatly reduced oxidation of Li foil upon the exposure to air. Similarly, larger F and S content is expected in thicker SEI films. However, higher F/C ratio observed at higher temperatures indicates higher concentration of dense ionically conductive salt decomposition products in the SEI compared to the concentration of organic species originating from the decomposed solvents.

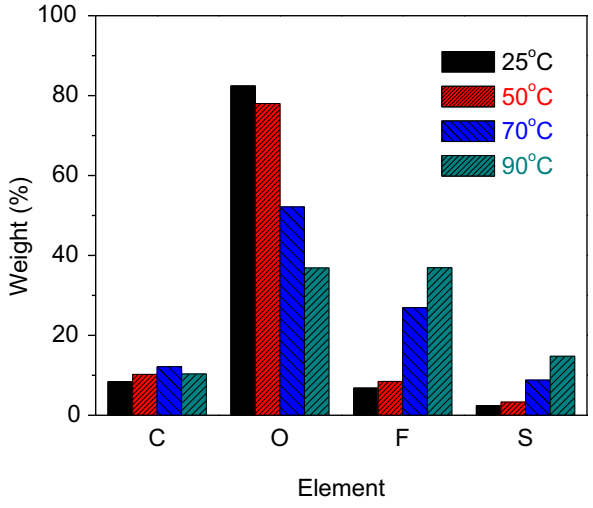

Fig. 10. EDS analysis showing the chemical composition of the SEI on the surface of Li anode cycled at different temperatures.

Significantly higher elastic modulus of inorganic components likely contributed to the observed reduction of Li dendrites on Li foil. The formation of dendrites during cycling is one of the biggest obstacles in the batteries using Li metal, since it can puncture the separator and short circuit the batteries. Therefore, the mitigation of the dendrite growth by the in-situ formation of the rigid SEI layer on Li at elevated temperatures could be an attractive strategy that could be explored to develop safe Li foil anodes in commercial cells. Higher conductivity of the SEI at higher temperatures likely counter-balanced its increased thickness (Figs. 8 and 9) and thus expectedly higher resistance, contributing to the high overall rate capability of the high temperature cells (Fig. 2).

Since temperature shall not affect the relative content of F and S among the LiTFSI decomposition products, the changes in the S/F ratio in the SEI shall indicate changes in the S dissolution with increasing temperature. In contrast to our initial expectation to observe higher S/F ratio at elevated temperatures, at which the dissolution of S cathodes shall be the fastest, we observe very little

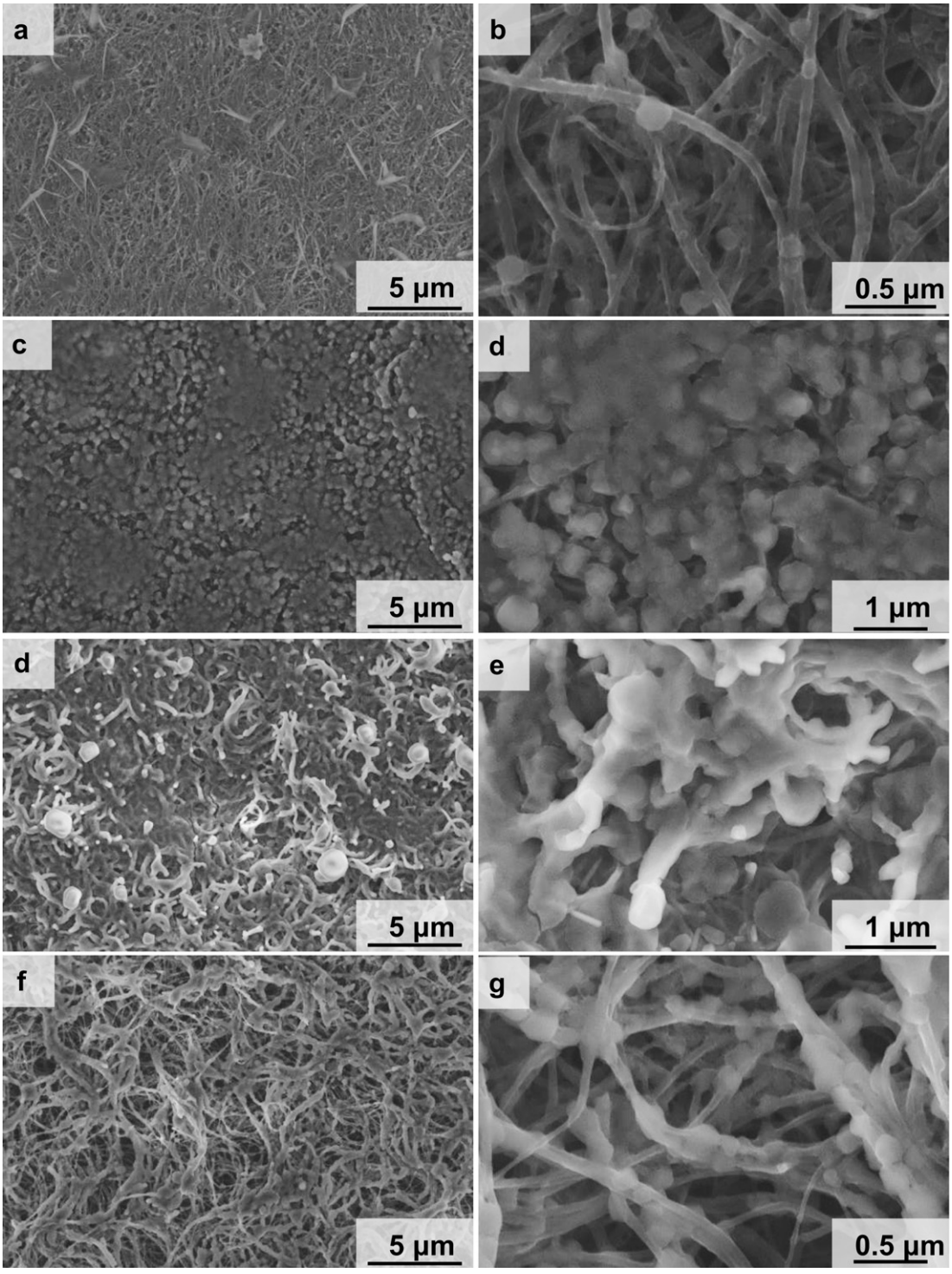

Fig. 11. SEM micrographs of S-CNT cathode after cycling at (a, b) 25 °C (c, d) 50 °C (e, f) 70 °C and (g) 90 °C.

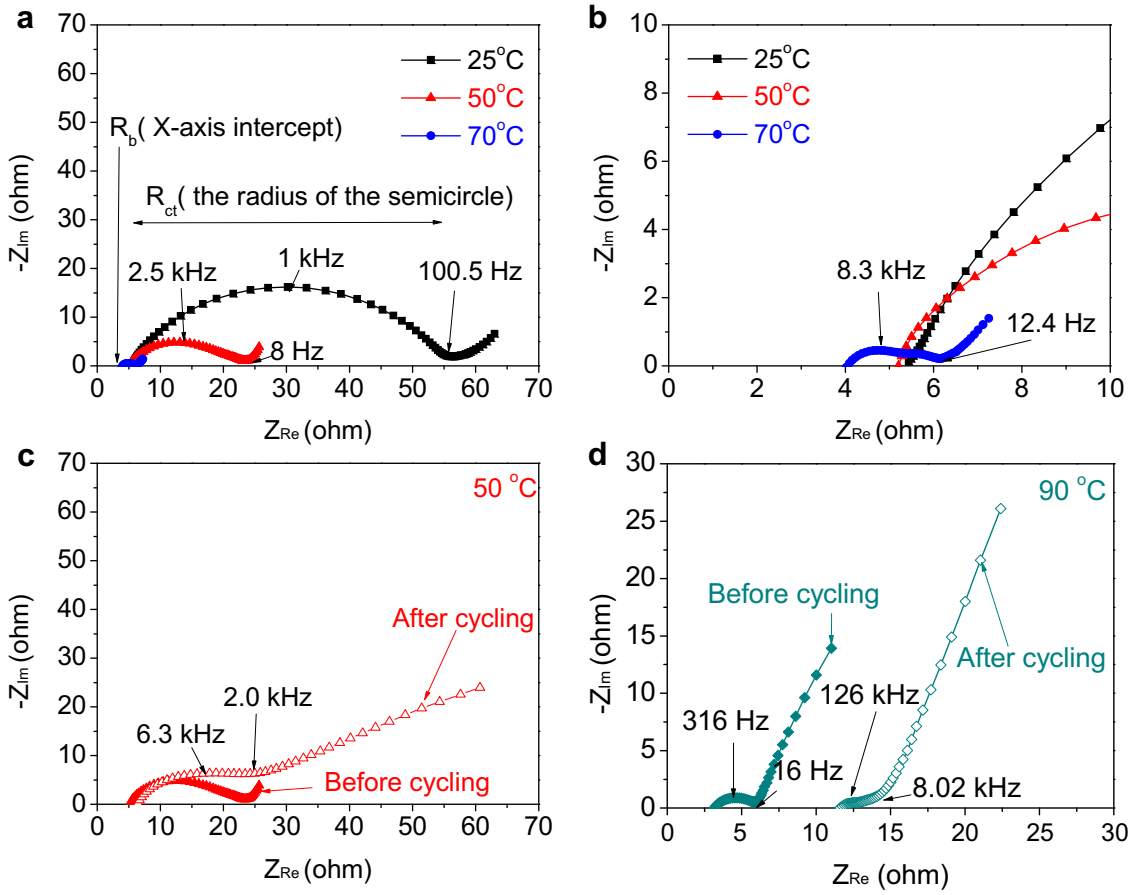

Fig. 12. Impedance spectroscopy. (a) The initial impedance before the cycling test at 25, 50 and 70 °C. (b) High frequency part of (a). (c) The change in impedance after 400 cycles at 2C-rate at 50 °C. (d) The change in impedance after 400 cycles at 2C-rate at 90 °C.

temperature dependence – the value of this ratio was 0.37 ± 0.4 (±10%) in all the samples. The lowest ratio (0.33) was observed in 70 °C cells. Our hypothesis is that thicker SEI prevents diffusion of the dissolved polysulfides onto the Li surface, while allowing the diffusion of smaller Li ions. As such, thicker SEI prevents the highly undesirable irreversible reduction and the precipitation of the polysulfides into Li_2S. We postulate this phenomenon to be responsible for longer cycle life and higher charge/discharge efficiency of cells cycled at 70 and 90 °C.

SEM studies of VACNT/S cathodes after cycling showed a major impact of cycling temperature on the morphological changes within the electrodes (Fig. 11). At 25 °C, only a small amount of reaction products were left on the electrode surface, as this S was lost irreversibly on Li anode during cycling. At 50 °C, spherical shaped LiS and/or Li_2S covered all over the top surface of the electrode, which likely explains its fast capacity degradation (Fig. 4). Indeed, the dissolved polysulfide during discharging must have diffused back and re-deposited primarily on the electrode top surface (Fig. 4d), blocking the access of the electrolyte to the bulk of the electrode and thus lowering sulfur utilization. At the highest temperature of 90 °C, the electrode remained porous and uniform (Fig. 4g). As the temperature was approaching the S melting point, the S coated CNT wall surface uniformly and nearly conformably, which greatly enhanced its utilization. At this temperature the polysulfide diffusion through the bulk of the CNT electrode and reversible re-deposition was very fast, preventing preferential re-deposition at the top electrode surface. Because the LiS and Li_2S were re-deposited on the CNT surface conformably, the electrode retained pathways for rapid electrolyte access, while maintaining the electrical connectivity. The morphology at 70 °C showed a transition stage between 50 and 90 °C (Fig. 4e).

Electrochemical impedance spectroscopy (EIS) was performed to see the changes in the cell resistance with the temperature. When Li–S cells were heated (Fig. 12a), both the charge transfer resistance (R_{ct}) and the bulk electrolyte/SEI resistance (R_b) was decreased probably due to the higher ionic conductivity and better wetting of the electrolyte through the electrode. EIS also detects changes in the SEI thickness over time in cells operating at different temperatures. While the R_b increased slightly by only 1.2Ω at 50 °C, it was increased by ~10Ω at 90 °C, as expected for significant SEI growth observed in high temperature cells. Interestingly, while the R_{ct} increased at 50 °C, the R_{ct} decreased during 90 °C cycling, suggesting improved SEI/wetting behavior on the S cathode surface for a more facile Li ion transport within the cathode.

4. Conclusions

Li–S batteries based on S nanoparticles uniformly distributed within VACNT current collector array were operated at elevated temperatures up to 90 °C in order to investigate the effect of high temperature on the cell capacity, rate capability and cycle durability. As increasing the temperature, both the capacity and rate capability improved due to the high ionic conductivity and better wetting of the electrolyte through the complicated electrode structure. The cycle life tests showed greatly enhanced cycle stability at 70 and 90 °C than at 25 and 50 °C. SEM and EDS studies revealed formation

of significantly thicker SEI on the Li anode surface at higher temperatures. The composition of inorganic components of this SEI was also found to increase with increasing temperature, resulting in the suppression of the Li dendrite growth. Thicker SEI on Li prevented diffusion of the polysulfides to active Li surface and their irreversible reduction into Li_2S, which was suggested to greatly enhance cell stability. When operating at 70 °C the cells demonstrated the best rate capability and capacities in the range excess of 500–700 mAh g_S^{-1} at the ultra-high current density of 3.3 A g_S^{-1}. At 90 °C Li–S cells showed initial fading followed by the increase in capacities to over 400 mAh g_S^{-1} and stable performance for 150 cycles. To the best of our knowledge the observed combination of high capacities and short charge-discharge time (6–7 min) in cathodes with relatively high mass loading ($\sim$1 mg cm^{-2}) is unprecedented. Considering S not being confined, the observed stability is quite remarkable and this finding suggests a great promise of the approach to form a stabilizing SEI on Li foil *in-situ*.

Acknowledgement

The authors would like to acknowledge the support of Carl Hinners (US Navy, China Lake, CA, USA) and thank Dr. Won Il Cho for a helpful discussion. Part of this research was also supported by the Energy Efficiency & Resources program of the Korea Institute of Energy Technology Evaluation and Planning (KETEP) grant funded by the Korea government Ministry of Knowledge Economy (20118510010030).

References

[1] B. Scrosati, J. Hassoun, Y.-K. Sun, Energy & Environmental Science 4 (2011) 3287–3295.
[2] Y. Idota, T. Kubota, A. Matsufuji, Y. Maekawa, T. Miyasaka, Science 276 (1997) 1395–1397.
[3] K. Kang, Y.S. Meng, J. Bréger, C.P. Grey, G. Ceder, Science 311 (2006) 977–980.
[4] P.L. Taberna, S. Mitra, P. Poizot, P. Simon, J.M. Tarascon, Nature Materials 5 (2006) 567–573.
[5] J.M. Tarascon, M. Armand, Nature 414 (2001) 359–367.
[6] J. Cabana, L. Monconduit, D. Larcher, M.R. Palacin, Advanced Materials 22 (2010) E170–E192.
[7] B.L. Ellis, K.T. Lee, L.F. Nazar, Chemistry of Materials 22 (2010) 691–714.
[8] C.K. Chan, H. Peng, G. Liu, K. McIlwrath, X.F. Zhang, R.A. Huggins, Y. Cui, Nature Nanotechnology 3 (2008) 31–35.
[9] I. Kovalenko, B. Zdyrko, A. Magasinski, B. Hertzberg, Z. Milicev, R. Burtovyy, I. Luzinov, G. Yushin, Science 334 (2011) 75–79.
[10] A. Magasinski, P. Dixon, B. Hertzberg, A. Kvit, J. Ayala, G. Yushin, Nature Materials 9 (2010) 353–358.
[11] K. Evanoff, A. Magasinski, J. Yang, G. Yushin, Advanced Energy Materials 1 (2011) 495–498.
[12] B. Hertzberg, A. Alexeev, G. Yushin, Journal of the American Chemical Society 132 (2010) 8548–8549.
[13] Y.S. Hu, R. Demir-Cakan, M.M. Titirici, J.O. Muller, R. Schlogl, M. Antonietti, J. Maier, Angewandte Chemie International Edition 47 (2008) 1645–1649.
[14] V. Baranchugov, E. Markevich, E. Pollak, G. Salitra, D. Aurbach, Electrochemistry Communications 9 (2007) 796–800.
[15] J.S. Bridel, T. Azais, M. Morcrette, J.M. Tarascon, D. Larcher, Chemistry of Materials 22 (2010) 1229–1241.
[16] H. Kim, B. Han, J. Choo, J. Cho, Angewandte Chemie International Edition 47 (2008) 10,151–10,154.
[17] J.C. Guo, C.S. Wang, Chemical Communications 46 (2010) 1428–1430.
[18] D. Mazouzi, B. Lestriez, L. Roue, D. Guyomard, Electrochemical and Solid State Letters 12 (2009) A215–A218.
[19] C. Liang, N.J. Dudney, J.Y. Howe, Chemistry of Materials 21 (2009) 4724–4730.
[20] J. Hassoun, B. Scrosati, Angewandte Chemie International Edition 49 (2010) 2371–2374.
[21] J. Wang, Y. Wang, X. He, J. Ren, C. Jiang, C. Wan, Journal of Power Sources 138 (2004) 271–273.
[22] N. Machida, K. Kobayashi, Y. Nishikawa, T. Shigematsu, Solid State Ionics 175 (2004) 247–250.
[23] P.G. Bruce, S.A. Freunberger, L.J. Hardwick, J.-M. Tarascon, Nature Materials 11 (2012) 19–29.
[24] X.L. Ji, S. Evers, R. Black, L.F. Nazar, Nature Communications 2 (2011).
[25] S.S. Zhang, D.T. Tran, Journal of Power Sources 211 (2012) 169–172.
[26] E. Peled, Y. Sternberg, A. Gorenshtein, Y. Lavi, Journal of the Electrochemical Society 136 (1989) 1621–1625.
[27] E. Peled, A. Gorenshtein, M. Segal, Y. Sternberg, Journal of Power Sources 26 (1989) 269–271.
[28] R. Elazari, G. Salitra, G. Gershinsky, A. Garsuch, A. Panchenko, D. Aurbach, Electrochemistry Communications 14 (2012) 21–24.
[29] R. Elazari, G. Salitra, A. Garsuch, A. Panchenko, D. Aurbach, Advanced Materials 23 (2011) 5641.
[30] J. Wang, J. Yang, C. Wan, K. Du, J. Xie, N. Xu, Advanced Functional Materials 13 (2003) 487–492.
[31] W. Zheng, Y.W. Liu, X.G. Hu, C.F. Zhang, Electrochimica Acta 51 (2006) 1330–1335.
[32] S. Li, M. Xie, J. Liu, H. Wang, H. Yan, Electrochemical and Solid-State Letters 14 (2011) A105–A107.
[33] H. Wang, Y. Yang, Y. Liang, J.T. Robinson, Y. Li, A. Jackson, Y. Cui, H. Dai, Nano Letters 11 (2011) 2644–2647.
[34] L. Yin, J. Wang, J. Yang, Y. Nuli, Journal of Materials Chemistry 21 (2011) 6807–6810.
[35] X. Ji, K.T. Lee, L.F. Nazar, Nature Materials 8 (2009) 500–506.
[36] J.C. Guo, Y.H. Xu, C.S. Wang, Nano Letters 11 (2011) 4288–4294.
[37] J.R. Akridge, Y.V. Mikhaylik, N. White, Solid State Ionics 175 (2004) 243–245.
[38] G. He, X.L. Ji, L. Nazar, Energy & Environmental Science 4 (2011) 2878–2883.
[39] X.L. Ji, K.T. Lee, L.F. Nazar, Nature Materials 8 (2009) 500–506.
[40] K. Evanoff, J. Khan, A.A. Balandin, A. Magasinski, W.J. Ready, T.F. Fuller, G. Yushin, Advanced Materials 24 (2012) 533.
[41] S. Dorfler, M. Hagen, H. Althues, J. Tubke, S. Kaskel, M.J. Hoffmann, Chemical Communications 48 (2012) 4097–4099.
[42] Y. Inoue, K. Kakihata, Y. Hirono, T. Horie, A. Ishida, H. Mimura, Applied Physics Letters 92 (2008).
[43] X. Liang, Z. Wen, Y. Liu, M. Wu, J. Jin, H. Zhang, X. Wu, Journal of Power Sources 196 (2011) 9839–9843.
[44] M. Wachtler, J.O. Besenhard, M. Winter, Journal of Power Sources 94 (2001) 189–193.
[45] D. Aurbach, E. Zinigrad, Y. Cohen, H. Teller, Solid State Ionics 148 (2002) 405–416.
[46] J.-I. Yamaki, S.-I. Tobishima, K. Hayashi, S. Keiichi, Y. Nemoto, M. Arakawa, Journal of Power Sources 74 (1998) 219–227.
[47] D. Aurbach, E. Pollak, R. Elazari, G. Salitra, C.S. Kelley, J. Affinito, Journal of the Electrochemical Society 156 (2009) A694–A702.